

X-ray frequency combs from optically controlled resonance fluorescence

Stefano M. Cavaletto,^{1,*} Zoltán Harman,^{1,2} Christian Buth,¹ and Christoph H. Keitel¹

¹*Max-Planck-Institut für Kernphysik, Saupfercheckweg 1, 69117 Heidelberg, Germany*

²*ExtreMe Matter Institute (EMMI), Planckstrasse 1, 64291 Darmstadt, Germany*

(Dated: February 14, 2013)

Abstract

An x-ray pulse-shaping scheme is put forward for imprinting an optical frequency comb onto the fluorescent radiation emitted on an atomic x-ray transition, thus producing an x-ray frequency comb. A four-level system is used to describe the level structure of N ions driven by small-bandwidth x rays, an optical laser field, and an optical frequency comb. By including many-particle constructive interference and the resulting enhancement of the emitted resonance fluorescence, a spectrum is predicted consisting of a frequency comb centered on the atomic x-ray transition energy and with the same tooth spacing as the driving optical frequency comb. This scheme paves the way towards the generation of x-ray frequency combs with energies from the 100-eV to the kiloelectronvolt range.

PACS numbers: 32.50.+d, 32.80.Qk, 42.50.Gy, 42.62.Eh

The introduction [1] and development [2] of optical frequency combs led to major advances in precision spectroscopy [3–5]. The spectrum of a frequency comb consists of a series of equally spaced teeth, namely, the modes of a train of femtosecond pulses spaced by the repetition frequency of a mode-locked laser. By counting the number of teeth between a known optical reference frequency and an unknown frequency, this comb is used as a very fine ruler to measure an optical frequency instead of the corresponding wavelength, which could be determined much less precisely. This allows one to reach relative accuracies up to 10^{-18} [6]. By precisely counting optical oscillations, e.g., in trapped atoms and trapped ions standards, optical frequency combs play a crucial role in the realization of all-optical atomic clocks [4, 7].

In light of the success of optical frequency-comb metrology, it is highly desirable to extend this technology to extreme ultraviolet (XUV) and x-ray frequencies [5]. X-ray frequency combs enable precise measurements of high-energy transitions that parallel the accuracy achieved for optical frequencies, thus representing an improvement of several orders of magnitude: this allows, to name but a few examples, even more stringent experimental tests of quantum electrodynamics and astrophysical models [8], and search for variability of the fine-structure constant, to which transitions in highly charged ions are predicted to be more sensitive [9]. One can also envision ultraprecise x-ray atomic clocks.

XUV frequency combs have been generated via intracavity high-order harmonic generation (HHG) [10]. While in conventional HHG an optical pulse in a gas produces a spectrum containing the odd harmonics of the optical frequency, in intracavity HHG a train of coherent optical pulses generates an HHG spectrum which in each harmonic line is structured into a fine comb. Based on this scheme, Ref. [11] reported the observation of frequency combs at ~ 40 nm (~ 30 eV). The required optical peak intensity of $\sim 10^{14}$ W/cm² was obtained with a femtosecond enhancement cavity. Yet relativistic effects set a maximum to the highest harmonic for which HHG operates efficiently [12].

In this Letter we develop a scheme of x-ray pulse shaping, by using an optical frequency comb to imprint its structure onto the resonance fluorescence spectrum emitted by an x-ray transition to produce an x-ray frequency comb. For this purpose we take advantage of previous investigations of many-color schemes of resonance fluorescence in multi-level systems [13, 14]. Examples of x-ray pulse shaping are, e.g., studies of electromagnetically induced transparency for x rays [15], for which an optical field is used to control x-ray absorption. Anticipated advances in small-bandwidth x-ray sources [16–18] will make our approach an attractive alternative, eventually able to reach, at relatively low optical-comb peak intensities, energies up to the kiloelectronvolt range.

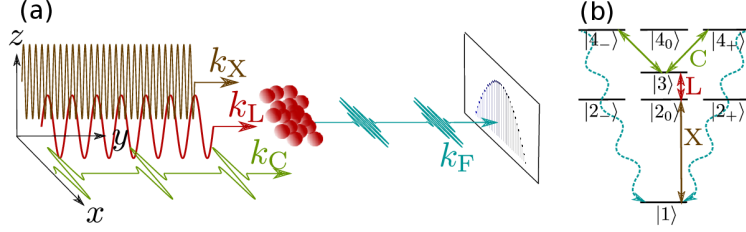


Figure 1. (Color online) (a) An ensemble of ions is driven by x rays (\mathbf{k}_X , brown), an auxiliary optical laser field (\mathbf{k}_L , red), both linearly polarized along the z direction, and an optical frequency comb (\mathbf{k}_C , green), linearly polarized along the x direction. All fields propagate in the y direction. The resonance fluorescence spectrum (\mathbf{k}_F , blue) exhibits an induced x-ray frequency-comb structure. (b) Four-level scheme used to describe the coherent interaction between He-like ions and the driving fields.

The geometry used is displayed in Fig. 1(a). An x-ray field $\mathcal{E}_X(\mathbf{r}, t)$, an optical auxiliary continuous-wave (cw) field $\mathcal{E}_L(\mathbf{r}, t)$, and an optical frequency comb $\mathcal{E}_C(\mathbf{r}, t)$, irradiate an ensemble of ions. The fields copropagate in the y direction; at time t and position \mathbf{r} , they are given by

$$\mathcal{E}_q(\mathbf{r}, t) = \mathcal{E}_{q,0}(t) \cos [\omega_q t + \varphi_q(t) + \varphi_{q,0} - \mathbf{k}_q \cdot \mathbf{r}] \hat{\mathbf{e}}_q, \quad (1)$$

with amplitude $\mathcal{E}_{q,0}(t)$, carrier frequency ω_q , phase $\varphi_q(t)$, carrier-envelope phase $\varphi_{q,0}$, wavevector $\mathbf{k}_q = (\omega_q/c) \hat{\mathbf{e}}_y$, linear polarization vector $\hat{\mathbf{e}}_q$, and intensity $I_q = |\mathcal{E}_{q,0}|^2/(8\pi\alpha)$ [19]. Furthermore, $\hat{\mathbf{e}}_X = \hat{\mathbf{e}}_L = \hat{\mathbf{e}}_z$, $\hat{\mathbf{e}}_C = \hat{\mathbf{e}}_x$, where $\hat{\mathbf{e}}_x$, $\hat{\mathbf{e}}_y$, and $\hat{\mathbf{e}}_z$ are the unit vectors in the x , y , and z direction, respectively; further, c is the speed of light and $\alpha = 1/c$ is the fine-structure constant. Atomic units are used throughout unless otherwise stated.

The optical bandwidth of $\mathcal{E}_L(\mathbf{r}, t)$ is so small that it can be entirely neglected. We first assume that $\mathcal{E}_X(\mathbf{r}, t)$ has constant amplitude, $\mathcal{E}_{X,0}(t) = \bar{\mathcal{E}}_{X,0}$, and constant phase, $\varphi_X(t) = 0$; the effect of the x-ray bandwidth is later taken into account through a stochastic approach [20]. Finally, the optical frequency comb has constant phase, $\varphi_C(t) \equiv 0$, and a periodic amplitude [21], $\mathcal{E}_{FC,0}(t) = \sum_{k=-\infty}^{+\infty} A_k e^{-i\frac{2\pi k}{T_p}t}$, with the Fourier coefficients $A_k = 1/T_p \int_0^{T_p} \mathcal{E}_{FC,0}(t) e^{i\frac{2\pi k}{T_p}t} dt$, i.e.,

$$\mathcal{E}_{FC,0}(t) = \mathcal{E}_{FC,max} \sum_{n=-\infty}^{+\infty} \mathcal{G}(t - nT_p), \quad (2a)$$

$$\mathcal{G}(t) = \cos^2 \left[\frac{\pi}{T_d} \left(t - \frac{T_d}{2} \right) \right] R \left[\frac{1}{T_d} \left(t - \frac{T_d}{2} \right) \right], \quad (2b)$$

where $\mathcal{E}_{FC,max} = \sqrt{8\pi\alpha I_{FC,max}}$ is its maximum, $I_{FC,max}$ the maximum intensity, and the rectangular function is defined with the help of the Heaviside step function θ as $R(x) = \theta(x + 1/2) - \theta(x - 1/2)$. The full width at half maximum (FWHM) of $\mathcal{G}^2(t)$ is $T_{FWHM} = 2T_d \arccos(\sqrt[4]{1/2})/\pi$ [22], with T_d being the interval in which $\mathcal{G}(t)$ is different from 0, $T_d \ll T_p$.

The electric fields $\mathcal{E}_X(\mathbf{r}, t)$, $\mathcal{E}_L(\mathbf{r}, t)$, and $\mathcal{E}_C(\mathbf{r}, t)$, are used to drive electric-dipole (E1) transitions in the four-level system depicted in Fig. 1(b), where level i has energy ω_i and the transition energy between the levels i and j is given by $\omega_{ij} = \omega_i - \omega_j$, $i, j \in \{1, 2_{0,\pm}, 3, 4_{0,\pm}\}$. The four-level model describes He-like ions, such as Be^{2+} and Ne^{8+} [23], with transition energies in the proper optical and x-ray ranges. Here the state $|1\rangle$ represents the ground state $1s^2 1S_0$, with total-angular-momentum quantum number $J = 0$ and positive parity. The three states $|2_-\rangle$, $|2_0\rangle$, and $|2_+\rangle$, with M_J equal to -1 , 0 , and 1 , respectively, describe the level $1s2p 3P_1$, with $J = 1$ and negative parity. Furthermore, $|3\rangle$ represents $1s2s 1S_0$, with $J = 0$ and positive parity, whereas the highest level $1s2p 1P_1$, with $J = 1$ and negative parity, is represented by the three states $|4_-\rangle$, $|4_0\rangle$, and $|4_+\rangle$. In He-like ions, level 3 has higher energy than level 2 for a nuclear charge $Z \geq 7$ [23] [Fig. 1(b)]; otherwise, these two levels are inverted in energy. Other levels, such as $1s2s 3S_1$, $1s2p 3P_0$, and $1s2p 3P_2$, are neglected entirely, since they do not couple via E1 interaction to the four levels in Fig. 1(b) and the spontaneous-decay times from higher-energy levels of Fig. 1(b) to them are by orders of magnitude lower than T_p . The excited levels 2, 3, and 4, are nonautoionizing, since in all configurations one electron occupies the $1s$ orbital, implying that the levels are energetically below the autoionizing threshold [23].

The interaction of the three electric fields $\mathcal{E}_q(\mathbf{r}, t)$ [Eq. (1)] with N ions at positions \mathbf{r}_n , for $n \in \{1, \dots, N\}$, is described by the Hamiltonian $\hat{H} = \hat{H}_0 + \sum_q \hat{H}_{\text{E1},q}$, where $\hat{H}_0 = \sum_{n=1}^N \sum_{i \in \{1, 2_{0,\pm}, 3, 4_{0,\pm}\}} \omega_i \hat{\sigma}_{ii}^n$ is the atomic electron-structure Hamiltonian and $\hat{H}_{\text{E1},q} = \sum_{n=1}^N \hat{\mathbf{d}}_n \cdot \mathcal{E}_q(\mathbf{r}_n, t)$ are the E1 interaction Hamiltonians [24, 25]. Here $\hat{\mathbf{d}}_n = \sum_{i,j \in \{1, 2_{0,\pm}, 3, 4_{0,\pm}\}} \mathbf{d}_{ij} \hat{\sigma}_{ij}^n$ is the n -ion, full electric-dipole moment operator, with $\mathbf{d}_{ij} = \langle i | \hat{\mathbf{d}}_n | j \rangle$ being its matrix elements and $\hat{\sigma}_{ij}^n$ the n -ion ladder operators. The fields are tuned to the respective transition energies, i.e., $\omega_X = \omega_{21}$, $\omega_L = |\omega_{32}|$, and $\omega_C = \omega_{43}$. The effect of a field on the other transitions to which it is not tuned is entirely negligible: the relevant interactions are highlighted in Fig. 1(b). As a result, the undriven states $|2_{\pm}\rangle$ and $|4_0\rangle$, for which the decay from higher-energy levels is by orders of magnitude smaller than the decay to the ground state $|1\rangle$, can be neglected as well.

The time evolution of the system obeys the master equation [24] $d\hat{\rho}/dt = -i[\hat{H}, \hat{\rho}] + \mathcal{L}[\hat{\rho}]$, where $\hat{\rho}(t)$ is the density matrix of the system, with elements $\rho_{ij}^n(t) = \langle \hat{\sigma}_{ji}^n(t) \rangle = \text{Tr}\{\hat{\sigma}_{ji}^n(t) \hat{\rho}\}$, and the Liouville operator $\mathcal{L}[\hat{\rho}]$ represents the norm-conserving spontaneous decay of the system,

$$\mathcal{L}[\hat{\rho}] = \sum_{\substack{i,j \in \{1, 2_0, 3, 4_{0,\pm}\} \\ \omega_i < \omega_j}} \sum_{n=1}^N -\frac{\Gamma_{ji}}{2} (\hat{\sigma}_{ji}^n \hat{\sigma}_{ij}^n \hat{\rho} + \hat{\sigma}_{ij}^n \hat{\rho} \hat{\sigma}_{ji}^n) + \text{h.c.}, \quad (3)$$

where the E1 decay rates are given by $\Gamma_{ji} = 4\omega_{ji}^3 \alpha^3 |\mathbf{d}_{ij}|^2 / 3$ [24]; norm-nonconserving terms such

as those from autoionization are absent. Further, for cw x-ray and optical fields, and an optical frequency comb, the equations of motion (EOMs) are periodic with period T_p : the master equation admits a periodic solution, $\hat{\rho}^{\text{eq}}(t) = \hat{\rho}^{\text{eq}}(t + T_p)$, that is asymptotically reached after turn-on effects have ceased.

Though undriven, the E1-allowed transition $4 \rightarrow 1$ undergoes spontaneous decay: because of the polarization of the driving fields (Fig. 1), these photons, decaying from states $|4_{\pm}\rangle$ with $M_J = \pm 1$ to the state $|1\rangle$ with $M_J = 0$, differ in energy and in polarization from those spontaneously decaying on the $2 \rightarrow 1$ transition. Here we compute the spectrum of resonance fluorescence emitted on the $4 \rightarrow 1$ transition with energy ω_{41} in the x-ray regime.

The spectrum of resonance fluorescence is the sum of a coherent and an incoherent part [24, 26, 27], whose space distribution and intensity are highly affected by many-ion effects. The light coherently emitted by many different ions, in fact, adds constructively in the \hat{e}_y forward direction, along which the three driving fields propagate; this implies an enhancement of the spectrum of resonance fluorescence proportional to N^2 along the preferential emission direction \hat{e}_y . Owing to the lack of constructive interference, though, the incoherent part of the spectrum does not undergo any many-particle coherent enhancement: it is only proportional to N and is distributed in space with a dipole radiation pattern displaying very low space directionality [27]. In the forward direction, resonance fluorescence is dominated by coherent emission, such that we can neglect the incoherent part of the spectrum. The quantum regression theorem and the Wiener-Khintchine theorem relate $\hat{\rho}^{\text{eq}}(t)$ to the spectrum of resonance fluorescence on the $4 \rightarrow 1$ transition [24, 26, 27], whose coherent part is

$$S_{41,14}^{\text{coh}}(r \hat{e}_y, \omega) = \frac{\omega_{41}^4 |\tilde{d}_{41}|^2}{2\pi^2 T_p c^3 r^2} N^2 \int_0^{T_p} \int_0^{\infty} 2 \mathbf{Re}[\varrho_{14+}^{\text{eq}}(t + \tau) \varrho_{4+1}^{\text{eq}}(t) e^{-i(\omega - \omega_{41})\tau}] d\tau dt, \quad (4)$$

where $\varrho_{14+}^{\text{eq}}(t) = \rho_{14+}^{\text{eq},n}(t) e^{-i[\omega_{41}t - (\mathbf{k}_x + \mathbf{k}_L + \mathbf{k}_C) \cdot \mathbf{r}_n]}$ is the relevant element of the slowly varying, n -independent, periodic density matrix $\hat{\rho}^{\text{eq}}(t)$, and $\tilde{d}_{41} = \mathbf{d}_{4+1} \cdot \hat{e}_{\sigma_-} = \mathbf{d}_{4-1} \cdot \hat{e}_{\sigma_+}$. Equation (4) contains constructive interference of the four allowed paths due to the four combinations $\varrho_{1j}^{\text{eq}}(t + \tau) \varrho_{j'1}^{\text{eq}}(t)$, with $j, j' \in \{4_-, 4_+\}$ [28]. The periodicity of $\varrho_{4+1}^{\text{eq}}(t)$ implies [26] that $S_{41,14}^{\text{coh}}(r \hat{e}_y, \omega)$ is constituted by a frequency comb centered on the x-ray frequency ω_{41} with the same tooth spacing as the driving

optical frequency comb,

$$S_{41,14}^{\text{coh}}(r \hat{\mathbf{e}}_y, \omega) = \sum_{m=-\infty}^{+\infty} \mathcal{S}_m \delta\left(\omega - \omega_{41} - \frac{2\pi m}{T_p}\right), \quad (5a)$$

$$\mathcal{S}_m = \frac{\omega_{41}^4 |\tilde{d}_{41}|^2}{\pi c^3 r^2} N^2 \left| \frac{1}{T_p} \int_0^{T_p} \varrho_{4+1}^{\text{eq}}(t) e^{i \frac{2\pi m}{T_p} t} dt \right|^2. \quad (5b)$$

Here, $S_{41,14}^{\text{coh}}(r \hat{\mathbf{e}}_y, \omega) d\omega dA$ represents the power detected in the energy interval $[\omega, \omega + d\omega]$ and in a surface element $dA = r^2 d\Omega \hat{\mathbf{e}}_y$ centered at $\mathbf{r} = r \hat{\mathbf{e}}_y$. Because of phase matching of the radiation scattered by different particles, the photons emitted in the forward direction are focused in a beam of mean area $\Delta A = 2\pi^2 c r^2 / (\omega_{41} L)$ [27], where L is the mean length of the ion sample. It follows that $P_m = \mathcal{S}_m 2\pi^2 c r^2 / (\omega_{41} L)$ is the power contained in the m th peak of the spectrum.

We aim at generating an x-ray frequency comb with (a) the same number of peaks, i.e., overall width, as the optical comb driving the ions, and (b) with emitted power comparable with that of present-day XUV combs generated via HHG [11]. The power in each peak P_m in the comb [Eq. (5b)] is proportional to the modulus squared of the m th Fourier coefficient of $\varrho_{4+1}^{\text{eq}}(t)$. The properties of a Fourier-series expansion [29] imply that the overall width of the spectrum is inversely proportional to the duration of $\varrho_{4+1}^{\text{eq}}(t)$. This means that, in order to guarantee a wide x-ray comb with as many teeth as in the driving optical one, $\varrho_{4+1}^{\text{eq}}(t)$ must have a pulse shape as short as that of the pulses in the optical comb, e.g., by vanishing in their absence. To this extent, we introduce the pulse area $Q = \int_0^{T_p} |\mathbf{d}_{34+}| \mathcal{E}_{\text{FC},0}(t) dt$: in the case of a pulse satisfying the condition $Q = 2n\pi$, the system performs an integer number of Rabi cycles [24], such that the population and coherences of the highest level in the system are brought back to 0 exactly at the end of the pulse [30, 31]. Conversely, for $Q \neq 2n\pi$ the interaction with the pulse is followed by a post-pulse-exposure spontaneous decay of the highest level. By properly choosing $I_{\text{FC,max}}$ to fulfill $Q = 2n\pi$, the population of the states $|4_{\pm}\rangle$ and the off-diagonal terms $\varrho_{4\pm 1}^{\text{eq}}(t)$ Rabi flop only in the presence of an optical-comb pulse: the emitted spectrum [Eq. (5)] is given by peaks whose power [Eq. (5b)] is the Fourier coefficient of a function which is different from 0 in an interval of duration T_{FWHM} , and has an overall width of the order of $2\pi/T_{\text{FWHM}}$. In this way, the long decay $\varrho_{4+1}^{\text{eq}}(t) \sim e^{-\Gamma_{41} t}$ which follows if the intensity is not properly chosen is suppressed: if such an exponential decay takes place, in fact, the amplitude of the peaks in the spectrum [Eq. (5b)] is dominated by the Fourier coefficients of the function $e^{-\Gamma_{41} t}$, resulting in a spectrum of smaller width, $\Gamma_{41} \ll 2\pi/T_{\text{FWHM}}$, and smaller number of relevant teeth.

In Fig. 2 we show results from our theory applied to He-like Be^{2+} ions. The total spontaneous-decay rates Γ_{ji} are calculated with `grasp2K` [33] and the transition energies $\omega_{21} = 121.9$ eV, $\omega_{23} =$

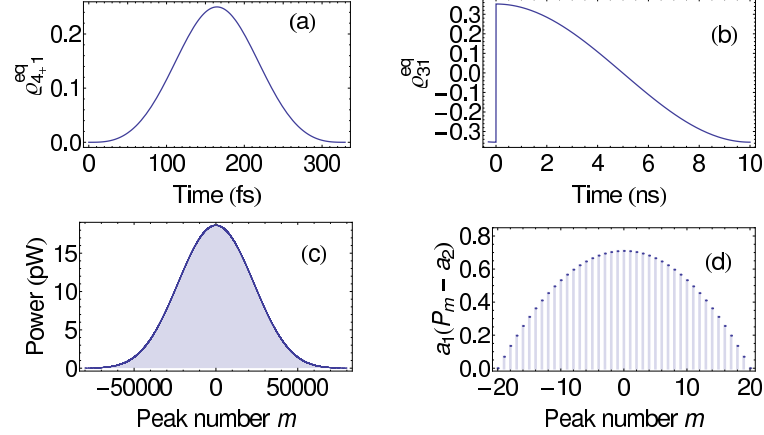


Figure 2. (Color online) Evolution in time of the elements of the density matrix $\hat{\rho}^{\text{eq}}(t)$ and spectrum of resonance fluorescence for Be^{2+} ions. Present-day parameters are used to model the driving optical frequency comb [Eq. (2)], $T_{\text{FWHM}} = 120$ fs, $T_p = 10$ ns, $1/T_p = 100$ MHz [11, 32], i.e., $2\pi/T_p = 4.1 \times 10^{-7}$ eV. The ion sample has $N = 10^6$ particles over a length $L = 1$ cm. The driving fields have intensities $I_X = 2.1 \times 10^2$ W/cm², $I_L = 1.7 \times 10^6$ W/cm², and $I_{C,\text{max}} = 3.0 \times 10^{10}$ W/cm², associated with a 2π optical frequency-comb pulse. The displayed periodic solutions are (a) $\rho_{4+1}^{\text{eq}}(t)$ for $nT_p < t < nT_p + T_d$, and (b) $\rho_{31}^{\text{eq}}(t)$ for $nT_p < t < (n+1)T_p$. The power P_m of each peak in the spectrum of Eq. (5) is displayed (c) for the whole comb, centered on $\omega_{41} = 123.7$ eV, and (d) around the maximum. In panel (d), $a_1 = 10^5$ pW⁻¹, $a_2 = 18.64$ pW.

0.2699 eV, $\omega_{43} = 2.018$ eV, and $\omega_{41} = 123.7$ eV, are taken from Ref. [23].

By using an optical frequency comb composed of 2π pulses to drive the $3 \leftrightarrow 4$ transition, population and coherences related to levels $|4_{\pm}\rangle$ vanish after each pulse. The time evolution of $\rho_{4+1}^{\text{eq}}(t)$ during a pulse is shown in Fig. 2(a). In the interval in between two optical frequency-comb pulses, when the highest states $|4_{\pm}\rangle$ are completely depopulated and undriven, the remaining three states $|1\rangle$, $|2_0\rangle$, and $|3\rangle$, behave as a three-level system [13] driven by the fields $\mathcal{E}_X(\mathbf{r}, t)$ and $\mathcal{E}_L(\mathbf{r}, t)$. During the interaction with a pulse from the optical frequency comb, the elements of the density matrix associated with these three states are brought to values, $\rho_{ij}^{\text{eq}}(T_d)$, which are different from the initial ones, $\rho_{ij}^{\text{eq}}(0)$, with $i, j \in \{1, 2_0, 3\}$. To guarantee the overall periodicity of the density matrix, $\hat{\rho}^{\text{eq}}(0) = \hat{\rho}^{\text{eq}}(T_p)$, one takes advantage of the Rabi inversion stimulated by the two fields $\mathcal{E}_X(\mathbf{r}, t)$ and $\mathcal{E}_L(\mathbf{r}, t)$, as shown in Fig. 2(b). A proper choice of the intensities I_X and I_L is therefore necessary, in order to maximize the peak of the periodic function $\rho_{4+1}^{\text{eq}}(t)$ and, correspondingly, the emitted photon number.

Having suppressed the post-pulse-exposure spontaneous decay of elements $\rho_{4+1}^{\text{eq}}(t)$, the corresponding spectrum of resonance fluorescence [Eq.(5)] is shown in Fig. 2(c): it is centered on

$\omega_{41} = 123.7$ eV and contains approximately 10^5 peaks of spacing $2\pi/T_p = 4.1 \times 10^{-7}$ eV. Figure 2(d) highlights the comb structure of the obtained spectrum. The necessary optical-comb peak intensity, $I_{FC,max} = 3.0 \times 10^{10}$ W/cm², is lower than those presently available and used for the generation of XUV frequency combs via HHG [32]. The power of each peak in the emitted spectrum—about tens of picowatts—is comparable with that measured in Ref. [11].

In order to incorporate the effect of the x-ray bandwidth γ_c , we adopt the approach developed in Ref. [20]. The x-ray field $\mathcal{E}_X(\mathbf{r}, t)$ is now a stochastic variable, varying in the ensemble of all possible realizations: one derives EOMs for the ensemble-averaged density matrix $\hat{\rho}^{eq,av}(t)$ to obtain the ensemble-averaged resonance fluorescence spectrum. We find that the δ -peak structure of Eq. (5) is now broadened and the spectrum consists of a continuous function whose peaks at $\omega_m = 2\pi m/T_p$ have a FWHM of $2\gamma_c$. In order to preserve the comb structure of Eq. (5), the bandwidth of the x-ray source must be smaller than the repetition frequency, i.e., $2\gamma_c < 2\pi/T_p = 4.1 \times 10^{-7}$ eV: the many-peak structure would otherwise disappear and the spectrum would reduce to a single wide peak. Such a small bandwidth is not available for x-ray frequencies at present. Yet one can weaken this condition by increasing the repetition frequency of the optical frequency comb $2\pi/T_p$, though this also results in a wider tooth spacing of the x-ray frequency comb. We notice, however, that the quality and coherence of x-ray light sources has dramatically improved during the last decades. In this respect, the advent of the x-ray free-electron laser (XFEL) [34] has raised encouraging prospects, e.g., self- or laser-seeding methods at XFELs [16] or the possibility to use an XFEL to drive an inner-shell x-ray laser [17, 18]. Advances in small-bandwidth x-ray sources are, therefore, expected to make our scheme a valid alternative for the generation of x-ray frequency combs.

In conclusion, we present a method for x-ray pulse shaping and use it to generate an x-ray frequency comb via the coherent interaction of an optical frequency comb in a multi-level system. We have applied our theory to He-like Be²⁺ at an x-ray energy of 123.7 eV and shown that the required peak intensity of the driving optical frequency comb compares with intensities from HHG-based methods. The scheme has general validity and can easily find use in modeling different physical systems. Qualitatively similar results can be obtained from other He-like ions, such as Ne⁸⁺; in this case, with $\omega_{41} = 922.0$ eV [23], we can predict a comb in the kiloelectronvolt range [35], yet for the transition energy $\omega_{43} = 6.679$ eV intense optical frequency combs are still not available. However, our model can be also applied to different atomic transitions, e.g., $1s^2 \rightarrow 1s np$ with $n \geq 3$ in heavier ions, for which experimentally accessible x-ray and optical energies can be found; or even to nuclear transitions up to the gamma range. Albeit relying on a driving x-ray field of high monochromaticity, our method will take advantage in the near future of the expected

advances in better-quality x-ray light sources; x-ray frequency combs will then enable to extend all the advantages of optical frequency-comb metrology up to the x-ray regime and allow for the development of the next-generation x-ray atomic clock.

The work of Z.H. was supported by the Alliance Program of the Helmholtz Association (HA216/EMMI).

* Corresponding author: smcavaletto@gmail.com

- [1] T. Udem, J. Reichert, R. Holzwarth, and T. W. Hänsch, [Opt. Lett. **24**, 881 \(1999\)](#); J. Reichert, R. Holzwarth, T. Udem, and T. W. Hänsch, [Opt. Commun. **172**, 59 \(1999\)](#).
- [2] T. Udem, J. Reichert, R. Holzwarth, and T. W. Hänsch, [Phys. Rev. Lett. **82**, 3568 \(1999\)](#); J. Reichert, M. Niering, R. Holzwarth, M. Weitz, T. Udem, and T. W. Hänsch, [Phys. Rev. Lett. **84**, 3232 \(2000\)](#); D. J. Jones, S. A. Diddams, J. K. Ranka, A. Stentz, R. S. Windeler, J. L. Hall, and S. T. Cundiff, [Science **288**, 635 \(2000\)](#); S. A. Diddams, D. J. Jones, J. Ye, S. T. Cundiff, J. L. Hall, J. K. Ranka, R. S. Windeler, R. Holzwarth, T. Udem, and T. W. Hänsch, [Phys. Rev. Lett. **84**, 5102 \(2000\)](#); M. Niering, R. Holzwarth, J. Reichert, P. Pokasov, T. Udem, M. Weitz, T. W. Hänsch, P. Lemonde, G. Santarelli, M. Abgrall, P. Laurent, C. Salomon, and A. Clairon, [Phys. Rev. Lett. **84**, 5496 \(2000\)](#); R. Holzwarth, T. Udem, T. W. Hänsch, J. C. Knight, W. J. Wadsworth, and P. S. J. Russell, [Phys. Rev. Lett. **85**, 2264 \(2000\)](#).
- [3] T. Udem, R. Holzwarth, and T. W. Hänsch, [Nature **416**, 233 \(2002\)](#); S. T. Cundiff and J. Ye, [Rev. Mod. Phys. **75**, 325 \(2003\)](#).
- [4] J. L. Hall, [Rev. Mod. Phys. **78**, 1279 \(2006\)](#).
- [5] T. W. Hänsch, [Rev. Mod. Phys. **78**, 1297 \(2006\)](#).
- [6] C. Orzel, [Physica Scripta **86**, 068101 \(2012\)](#).
- [7] S. A. Diddams, T. Udem, J. C. Bergquist, E. A. Curtis, R. E. Drullinger, L. Hollberg, W. M. Itano, W. D. Lee, C. W. Oates, K. R. Vogel, and D. J. Wineland, [Science **293**, 825 \(2001\)](#).
- [8] S. Bernitt, G. V. Brown, J. K. Rudolph, R. Steinbrugge, A. Graf, M. Leutenegger, S. W. Epp, S. Eberle, K. Kubicek, V. Mackel, M. C. Simon, E. Trabert, E. W. Magee, C. Beilmann, N. Hell, S. Schippers, A. Muller, S. M. Kahn, A. Surzhykov, Z. Harman, C. H. Keitel, J. Clementson, F. S. Porter, W. Schlotter, J. J. Turner, J. Ullrich, P. Beiersdorfer, and J. R. C. Lopez-Urrutia, [Nature **492**, 225 \(2012\)](#).
- [9] J. C. Berengut, V. A. Dzuba, V. V. Flambaum, and A. Ong, [Phys. Rev. Lett. **106**, 210802 \(2011\)](#).
- [10] R. J. Jones, K. D. Moll, M. J. Thorpe, and J. Ye, [Phys. Rev. Lett. **94**, 193201 \(2005\)](#); C. Gohle, T. Udem, M. Herrmann, J. Rauschenberger, R. Holzwarth, H. A. Schuessler, F. Krausz, and T. W. Hänsch, [Nature **436**, 234 \(2005\)](#).
- [11] A. Cingöz, D. C. Yost, T. K. Allison, A. Ruehl, M. E. Fermann, I. Hartl, and J. Ye, [Nature **482**, 68 \(2012\)](#).

[12] M. C. Kohler, T. Pfeifer, K. Z. Hatsagortsyan, and C. H. Keitel, in *Advances in Atomic, Molecular, and Optical Physics*, Vol. 61, edited by P. Berman, E. Arimondo, and C. Lin (Academic Press, New York, 2012) pp. 159 – 208.

[13] L. M. Narducci, M. O. Scully, G.-L. Oppo, P. Ru, and J. R. Tredicce, *Phys. Rev. A* **42**, 1630 (1990); A. S. Manka, H. M. Doss, L. M. Narducci, P. Ru, and G.-L. Oppo, *Phys. Rev. A* **43**, 3748 (1991).

[14] S.-Y. Zhu and M. O. Scully, *Phys. Rev. Lett.* **76**, 388 (1996); P. Zhou and S. Swain, *Phys. Rev. Lett.* **77**, 3995 (1996); E. Paspalakis and P. L. Knight, *Phys. Rev. Lett.* **81**, 293 (1998); C. H. Keitel, *Phys. Rev. Lett.* **83**, 1307 (1999); M. Macovei and C. H. Keitel, *Phys. Rev. Lett.* **91**, 123601 (2003); M. Kiffner, M. Macovei, J. Evers, and C. H. Keitel, in *Prog. Opt.*, Vol. 55, edited by E. Wolf (2010) Chap. 3, p. 85; O. Postavaru, Z. Harman, and C. H. Keitel, *Phys. Rev. Lett.* **106**, 033001 (2011).

[15] C. Buth, R. Santra, and L. Young, *Phys. Rev. Lett.* **98**, 253001 (2007); T. E. Glover, M. P. Hertlein, S. H. Southworth, T. K. Allison, J. van Tilborg, E. P. Kanter, B. Krassig, H. R. Varma, B. Rude, R. Santra, A. Belkacem, and L. Young, *Nature Physics* **6**, 69 (2010).

[16] J. Amann, W. Berg, V. Blank, F.-J. Decker, Y. Ding, P. Emma, Y. Feng, J. Frisch, D. Fritz, J. Hastings, Z. Huang, J. Krzywinski, R. Lindberg, H. Loos, A. Lutman, H.-D. Nuhn, D. Ratner, J. Rzepiela, D. Shu, Y. Shvyd'ko, S. Spampinati, S. Stoupin, S. Terentyev, E. Trakhtenberg, D. Walz, J. Welch, J. Wu, A. Zholents, and D. Zhu, *Nature Photonics* **6**, 693 (2012).

[17] N. Rohringer, D. Ryan, R. A. London, M. Purvis, F. Albert, J. Dunn, J. D. Bozek, C. Bostedt, A. Graf, R. Hill, S. P. Hau-Riege, and J. J. Rocca, *Nature* **481**, 488 (2012).

[18] G. Darvasi, C. H. Keitel, and C. Buth, submitted, (2013); C. Buth, M. C. Kohler, J. Ullrich, and C. H. Keitel, *Opt. Lett.* **36**, 3530 (2011).

[19] J. C. Diels and W. Rudolph, *Ultrashort laser pulse phenomena: fundamentals, techniques, and applications on a femtosecond time scale* (Academic Press, San Diego, London, 2006).

[20] G. S. Agarwal, *Phys. Rev. Lett.* **37**, 1383 (1976).

[21] The function is periodic in a very large time interval $T_g \gg T_p$, i.e., $\mathcal{E}_{FC,0}(t) = f(t) \sum_{n=-\infty}^{+\infty} A_n e^{-i \frac{2\pi n}{T_p} t}$, with $f(t) \approx 1$, $-T_g/2 < t < T_g/2$.

[22] I. Barth and C. Lasser, *J. Phys. B* **42**, 235101 (2009).

[23] V. A. Yerokhin and K. Pachucki, *Phys. Rev. A* **81**, 022507 (2010).

[24] M. O. Scully and S. Zubairy, *Quantum Optics* (Cambridge University Press, Cambridge, 1997).

[25] W. R. Johnson, *Atomic Structure Theory: Lectures on Atomic Physics* (Springer, Berlin Heidelberg, New York, 2007).

[26] M. A. Newbold and G. J. Salamo, *Phys. Rev. A* **22**, 2098 (1980).

[27] J. H. Eberly and M. V. Fedorov, *Phys. Rev. A* **45**, 4706 (1992); F. I. Gauthey, C. H. Keitel, P. L. Knight, and A. Maquet, *Phys. Rev. A* **52**, 525 (1995).

[28] M. Kiffner, J. Evers, and C. H. Keitel, *Phys. Rev. Lett.* **96**, 100403 (2006); *Phys. Rev. A* **73**, 063814 (2006).

[29] G. Arfken, H. Weber, and F. Harris, *Mathematical Methods for Physicists: A Comprehensive Guide* (Academic Press, Waltham, Oxford, 2011).

[30] N. Rosen and C. Zener, *Phys. Rev.* **40**, 502 (1932); A. Bambini and P. R. Berman, *Phys. Rev. A* **23**, 2496 (1981); K. Rzążewski and M. Florjańczyk, *J. Phys. B* **17**, L509 (1984).

[31] R. T. Robiscoe, *Phys. Rev. A* **17**, 247 (1978); M. Lewenstein, J. Zakrzewski, and K. Rzążewski, *J. Opt. Soc. Am. B* **3**, 22 (1986); S. M. Cavaletto, C. Buth, Z. Harman, E. P. Kanter, S. H. Southworth, L. Young, and C. H. Keitel, *Phys. Rev. A* **86**, 033402 (2012).

[32] I. Hartl, T. R. Schibli, A. Marcinkevičius, D. C. Yost, D. D. Hudson, M. E. Fermann, and J. Ye, *Opt. Lett.* **32**, 2870 (2007); T. R. Schibli, I. Hartl, D. C. Yost, M. J. Martin, A. Marcinkevičius, M. E. Fermann, and J. Ye, *Nature Photonics* **2**, 355 (2008); T. Eidam, S. Hanf, E. Seise, T. V. Andersen, T. Gabler, C. Wirth, T. Schreiber, J. Limpert, and A. Tünnermann, *Opt. Lett.* **35**, 94 (2010); A. Ruehl, A. Marcinkevičius, M. E. Fermann, and I. Hartl, *Opt. Lett.* **35**, 3015 (2010).

[33] P. Jönsson, X. He, C. Froese Fischer, and I. P. Grant, *Comput. Phys. Commun.* **177**, 597 (2007).

[34] P. Emma, R. Akre, J. Arthur, R. Bionta, C. Bostedt, J. Bozek, A. Brachmann, P. Bucksbaum, R. Cofee, F.-J. Decker, Y. Ding, D. Dowell, S. Edstrom, A. Fisher, J. Frisch, S. Gilevich, J. Hastings, G. Hays, P. Hering, Z. Huang, R. Iverson, H. Loos, M. Messerschmidt, A. Miahnahri, S. Moeller, H.-D. Nuhn, G. Pile, D. Ratner, J. Rzepiela, D. Schultz, T. Smith, P. Stefan, H. Tompkins, J. Turner, J. Welch, W. White, J. Wu, G. Yocky, and J. Galayda, *Nature Photonics* **4**, 641 (2010); W. Ackermann, G. Asova, V. Ayvazyan, A. Azima, N. Baboi, J. Bähr, V. Balandin, B. Beutner, A. Brandt, A. Bolzmann, R. Brinkmann, O. I. Brovko, M. Castellano, P. Castro, L. Catani, E. Chiadroni, S. Choroba, A. Cianchi, J. T. Costello, D. Cubaynes, J. Dardis, W. Decking, H. Delsim-Hashemi, A. Delserieys, G. Di Pirro, M. Dohlus, S. Düsterer, A. Eckhardt, H. T. Edwards, B. Faatz, J. Feldhaus, K. Flöttmann, J. Frisch, L. Fröhlich, T. Garvey, U. Gensch, C. Gerth, M. Görler, N. Golubeva, H.-J. Grabosch, M. Grecki, O. Grimm, K. Hacker, U. Hahn, J. H. Han, K. Honkavaara, T. Hott, M. Hünig, Y. Ivanisenko, E. Jaeschke, W. Jalmuzna, T. Jezynski, R. Kammering, V. Katalev, K. Kavanagh, E. T. Kennedy, S. Khodyachykh, K. Klose, V. Kocharyan, M. Körfer, M. Kollewe, W. Koprek, S. Korpanov, D. Kostin, M. Krassilnikov, G. Kube, M. Kuhlmann, C. L. S. Lewis, L. Lilje, T. Limberg, D. Lipka, F. Löhl, H. Luna, M. Luong, M. Martins, M. Meyer, P. Michelato, V. Miltchev, W. D. Möller, L. Monaco, W. F. O. Müller, O. Napieralski, O. Nopoly, P. Nicolosi, D. Nölle, T. Nuñez, A. Oppelt, C. Pagani, R. Paparella, N. Pchalek, J. Pedregosa-Gutierrez, B. Petersen, B. Petrosyan, G. Petrosyan, L. Petrosyan, J. Pflüger, E. Plönjes, L. Poletto, K. Pozniak, E. Prat, D. Proch, P. Pucyk, P. Radcliffe, H. Redlin, K. Rehlich, M. Richter, M. Roehrs, J. Roensch, R. Romaniuk, M. Ross, J. Rossbach, V. Rybníkov, M. Sachwitz, E. L. Saldin, W. Sandner, H. Schlarb, B. Schmidt, M. Schmitz, P. Schmüser, J. R. Schneider, E. A. Schneidmiller, S. Schnepp, S. Schreiber, M. Seidel, D. Sertore, A. V. Shabunov, C. Simon, S. Simrock, E. Sombrowski, A. A. Sorokin, P. Spanknebel, R. Spesyvtsev, L. Staykov, B. Steffen, F. Stephan, F. Stulle, H. Thom, K. Tiedtke, M. Tischer, S. Toleikis, R. Treusch, D. Trines, I. Tsakov, E. Vogel, T. Weiland, H. Weise, M. Wellhöfer, M. Wendt, I. Will, A. Winter, K. Wittenburg,

W. Wurth, P. Yeates, M. V. Yurkov, I. Zagorodnov, and K. Zapfe, *Nature Photonics* **1**, 336 (2007); D. Pile, *Nature Photonics* **5**, 456 (2011); M. Altarelli, R. Brinkmann, M. Chergui, W. Decking, B. Dobson, S. Düsterer, G. Grübel, W. Graeff, H. Graafsma, J. Hajdu, J. Marangos, J. Pflüger, H. Redlin, D. Riley, I. Robinson, J. Rossbach, A. Schwarz, K. Tiedtke, T. Tschentscher, I. Vartaniants, H. Wabnitz, H. Weise, R. Wichmann, K. Witte, A. Wolf, M. Wulff, and M. Yurkov, *The European X-Ray Free-Electron Laser, Technical Design Report*, Tech. Rep. (DESY, Hamburg, Germany, 2006).

[35] S. M. Cavaletto, Z. Harman, C. Buth, and C. H. Keitel, in preparation, (2013).